Supplementary Information: $BaCuS_2$: a superconductor with moderate electron-electron correlation

Yuhao Gu,[1] Xianxin Wu,[1] Kun Jiang,[1] and Jiangping Hu[1,2,*]

[1]*Beijing National Laboratory for Condensed Matter Physics, and Institute of Physics, Chinese Academy of Sciences, Beijing 100190, China*

[2]*CAS Center of Excellence in Topological Quantum Computation and Kavli Institute of Theoretical Sciences, University of Chinese Academy of Sciences, Beijing 100190, China*

I. COMPUTATIONAL METHODS

Our electronic structure calculations employ the Vienna ab initio simulation package (VASP) code[1] with the projector augmented wave (PAW) method[2]. The Perdew-Burke-Ernzerhof (PBE)[3] exchange-correlation functional is used in our calculations. The kinetic energy cutoff is set to be 600 eV for the expanding the wave functions into a plane-wave basis in VASP calcuations. For body centered tetragonal $La_3N_3Ni_2B_2$ and $Ba_3Cu_2S_5$, we employ their primitive cells to perform calculations. In the calculations of the formation energy, the energy convergence criterion is 10^{-6} eV and the force convergence criterion is 0.01 eV/Å. The Γ-centered **k**-meshes are $16\times16\times8$, $6\times6\times6$, $16\times16\times16$, $18\times18\times4$, $18\times18\times22$, $20\times20\times12$ and $8\times8\times8$ for $BaCuS_2$, $Ba_3Cu_2S_5$, BaS, CuS, $CaCuO_2$, FeSe and $La_3N_3Ni_2B_2$, respectively.

We employ Wannier90[4, 5] to calculate maximally localized Wannier functions in $BaCuS_2$, $CaCuO_2$, FeSe and $La_3N_3Ni_2B_2$. In the calculations of the d-p models, the initial projectors are transition metal atoms' d-orbitals and anions' p-orbitals in $BaCuS_2$, $CaCuO_2$ and FeSe. For $La_3N_3Ni_2B_2$, the Ni(d)-B(p) valence manifold strongly entangles with other bands, so La's d-orbitals and B's s-orbitals are added in its initial projectors to reproduce DFT-calculated band structures. In the calculation of the d-p σ^* MLWFs, the initial projectors are Cu's $d_{x^2-y^2}+d_{z^2}$ orbitals in $BaCuO_2$ and Cu's $d_{x^2-y^2}$ orbital in $CaCuO_2$, respectively.

We employ EPW package[6] to calculate the electron-phonon coupling properties of $BaCuS_2$. The MLWFs are calculated by Wannier90[4, 5] interfacing with Quantum ESPRESSO[7]. We take the $16\times16\times8$ **k**-mesh and $4\times4\times2$ **q**-mesh as coarse grids and then interpolate to the $64\times64\times32$ **k**-mesh and $8\times8\times4$ **q**-mesh. The kinetic energy cutoff is set to 80 Ry. The Gaussian smearing method with the width of 0.005 Ry is used for the Fermi surface broadening. The energy convergence criterion is 10^{-12} eV. In the highly accurate structural optimization, the lattice constants and atomic coordinates are relaxed and the force convergence criterion is 0.000001 Ry/Bohr. The exchange-correlation functional is also PBE and the norm-conserving SG15 pseudopotentials are used[8–10].

* jphu@iphy.ac.cn

II. ELECTRON-PHONON PROPERTIES OF $BaCuS_2$

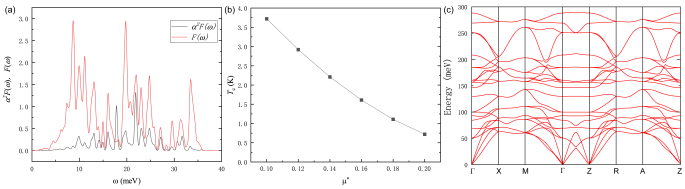

FIG. S1. (a) Eliashberg spectral function $\alpha^2F(\omega)$ (red line) and Phonon density of states $F(\omega)$ (black line) for $BaCuS_2$. (b) Evaluated T_c as a function of μ^* for $BaCuS_2$. (c) The phonon dispersion for $BaCuS_2$.

The phonon density of states $F(\omega)$ and the corresponding Eliashberg spectral function $\alpha^2F(\omega)$ are plotted in FIG.S1.(a). By intergating $\alpha^2F(\omega)$, we get a moderate EPC strength $\lambda = 0.59$. We estimate the superconducting transition temperature T_c with the McMillan-Allen-Dynes formula[11, 12],

$$T_c = \frac{\omega_{\log}}{1.2}\exp\left[\frac{-1.04(1+\lambda)}{\lambda\left(1-0.62\mu^*\right)-\mu^*}\right], \tag{1}$$

where μ^* is the effective screened Coulomb repulsion constant and the logarithmic average of the Eliashberg spectral function $\omega_{\log}$ is denfined as

$$\omega_{\log} = \exp\left[\frac{2}{\lambda}\int\frac{d\omega}{\omega}\alpha^2F(\omega)\ln(\omega)\right]. \tag{2}$$

As μ^* is an input parameter, we plot T_c as a function of μ^* in FIG.S1.(b). The phonon-mediated T_c for $BaCuS_2$ should be less than 4 K.

III. $Ba_3Cu_2S_5$: SEPARATION BY THREE ROCK SALT-TYPE BAS LAYERS

As shown in FIG.S2, the crystal structure of $Ba_3Cu_2S_5$ is similar to that of $BaCuS_2$: The inverse α-PbO-type Cu_2S_2 layer is separated by 3 rock salt-type BaS layers in $Ba_3Cu_2S_5$ but separated by 2 BaS layers in $BaCuS_2$ ($Ba_2Cu_2S_4$). It also shares a similar electronic structure with $BaCuS_2$, as shown in FIG.S2.(b). $Ba_3Cu_2S_5$ is not thermodynamically stable, but it is possible to synthesized $Ba_3Cu_2S_5$ under external pressure due to Cu's five-coordination, as shown in FIG.**??**.(a).

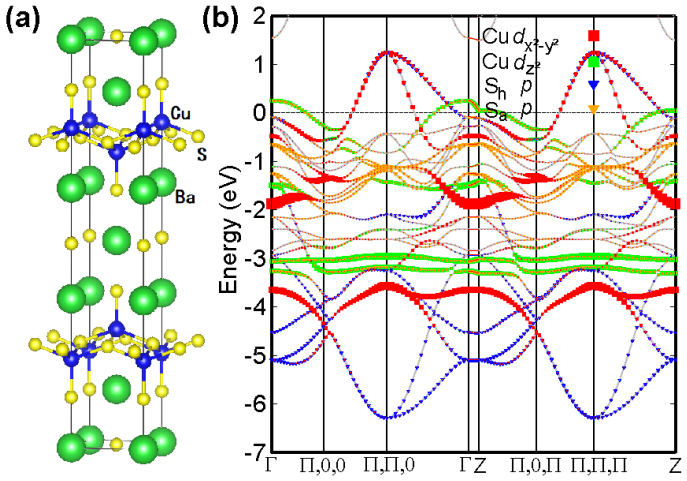

FIG. S2. (a) The crystal structure of $Ba_3Cu_2S_5$. (b) The band structure of $BaCuS_2$ with its primitive cell from DFT calculation. The sizes of dots represent the weights of the projection. Here S_a represents the apical S atoms while S_h represents the horizontal S atoms. The choice of the **k**-path is same as the literature's[13].

IV. WANNIERIZATION PROJECTED BY d-ORBITALS AND p-orbitals

Our Wannierization results successfully reproduce DFT-calculated band structures, as shown in FIG.S3. The relevant representative hopping parameters and on-site energies are listed in TABLE.S1. Here we use the conventional notations of the local crystal field coordinations.

TABLE S1. The hopping parameters and on-site energies for $BaCuS_2$, $CaCuO_2$, FeSe and $La_3N_3Ni_2B_2$. Here S_a represents the apical S atoms while S_h represents the horizontal S atoms.

$BaCuS_2$	
$\varepsilon_{Cu,d_{z2}}$	-2.21
$\varepsilon_{Cu,d_{x^2-y^2}}$	-2.23
$\varepsilon_{Cu,d_{xz/yz}}$	-2.32
$\varepsilon_{Cu,d_{xy}}$	-2.48
ε_{S_h,p_z}	-2.58
$\varepsilon_{S_h,p_{x/y}}$	-3.08
ε_{S_a,p_z}	-2.17
$\varepsilon_{S_a,p_{x/y}}$	-1.40
$\lvert t_{Cu,d_{x^2-y^2}-S_h,p_z}\rvert$	0.37
$\lvert t_{Cu,d_{x^2-y^2}-S_h,p_{x/y}}\rvert$	0.69
$\lvert t_{Cu,d_{z^2}-S_h,p_z}\rvert$	0.39
$\lvert t_{Cu,d_{z^2}-S_h,p_{x/y}}\rvert$	0.11
$\lvert t_{Cu,d_{z^2}-S_a,p_z}\rvert$	0.82
$\lvert t_{S_a,p_x-S_a,p_x}\rvert$	0.09
$CaCuO_2$	
$\varepsilon_{Cu,d_{z2}}$	-2.42
$\varepsilon_{Cu,d_{x^2-y^2}}$	-1.92
ε_{O,p_z}	-2.58
$\varepsilon_{O,p_{x/y}}$	-3.83
$\lvert t_{Cu,d_{x^2-y^2}-O,p_{x/y}}\rvert$	1.24
FeSe	
$\varepsilon_{Fe,d_{x^2-y^2}}$	-0.88
$\varepsilon_{Fe,d_{xz/yz}}$	-0.78
ε_{Se,p_z}	-3.07
$\varepsilon_{Se,p_{x/y}}$	-3.09
$\lvert t_{Fe,d_{x^2-y^2}-Se,p_{x/y}}\rvert$	0.25
$\lvert t_{Fe,d_{x^2-y^2}-Se,p_z}\rvert$	0.72
$\lvert t_{Fe,d_{xz/yz}-Se,p_{x/y}}\rvert$	1.00
$\lvert t_{Fe,d_{x^2-y^2}-Se,p_z}\rvert$	0.16
$La_3N_3Ni_2B_2$	
$\varepsilon_{Ni,d_{z2}}$	-2.11
$\varepsilon_{Ni,d_{x^2-y^2}}$	-2.26
$\varepsilon_{Ni,d_{xz/yz}}$	-2.11
$\varepsilon_{Ni,d_{xy}}$	-2.24
$\varepsilon_{B,s}$	0.23
ε_{B,p_z}	2.17
$\varepsilon_{B,p_{x/y}}$	0.28
$\lvert t_{Ni,d_{x^2-y^2}-Ni,p_{x/y}}\rvert$	0.55
$\lvert t_{Ni,d_{x^2-y^2}-Ni,p_z}\rvert$	0.78
$\lvert t_{Ni,d_{xz/yz}-Ni,p_{x/y}}\rvert$	0.85
$\lvert t_{Ni,d_{x^2-y^2}-Ni,p_z}\rvert$	0.27

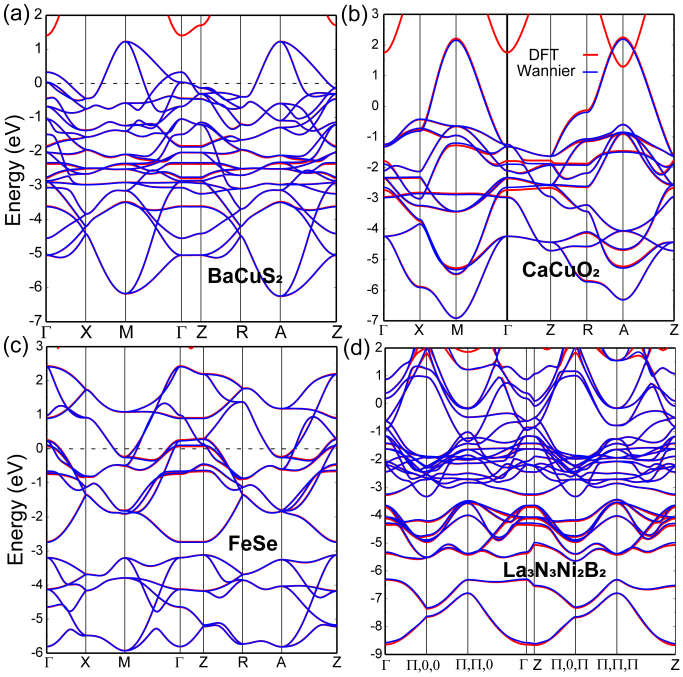

FIG. S3. The band structures of (a) $BaCuS_2$, (b) $CaCuO_2$, (c) FeSe and (d) $La_3N_3Ni_2B_2$. The red/blue lines represent DFT/Wannierization results, respectively. The choice of the **k**-path in (d) is same as the literature's[13].

V. WANNIERIZATION OF THE d-p σ^*-BONDING BANDS AND THE EFFECTIVE TIGHT-BINDING MODEL

As mentioned above, the in-plane d-p σ^*-bonding bands are isolated around the Fermi surface. In order to construct the effective minimal model to describe the in-plane electronic physics in $BaCuS_2$, we downfold the full $d-p$ model into an effective minimal model[14] by only Wannierizing the $d_{x^2-y^2}$-like and d_{z^2}-like MLWFs in $BaCuS_2$ with a smaller energy window. Our Wannierization results capture the main characters of $BaCuS_2$'s electronic structure, as shown in FIG.S4.(a). This is an analogy to the Zhang-Rice singlet in cuprates[15], so we also calculate the $d_{x^2-y^2}$-like MLWF in $CaCuO_2$ for comparison, as shown in FIG.S4.(b).

We construct the effective tight-binding (TB) model in the basis of $d_{x^2-y^2}$ orbital and d_{z^2} orbital to describe the in-plane electronic physics. Since there are two Cu atoms in one unit cell, the TB model can be written as a 4×4 Hermitian matrix:

$$
\begin{aligned}
H_{11} &= H_{33} = \varepsilon_1 + 2t_{11}^{x}(cos(k_x)+cos(k_y)) + 2t_{11}^{xx}(cos(2k_x)+cos(2k_y)) + 4t_{11}^{xxyy}(cos(k_x)cos(k_y)),\\
H_{12} &= H_{34} = 2t_{12}^{x}(cos(k_x)-cos(k_y)) + 2t_{12}^{xx}(cos(2k_x)-cos(2k_y)),\\
H_{13} &= 4t_{13}^{xy}cos(k_x/2)cos(k_y/2) + 4t_{13}^{xxy}(cos(k_x/2)*cos(3k_y/2)+cos(3k_x/2)cos(k_y/2)),\\
H_{14} &= H_{23} = 4t_{14}^{xxy}(cos(3k_x/2)cos(k_y/2)-cos(k_x/2)cos(3k_y/2)),\\
H_{22} &= H_{44} = \varepsilon_2 + 2t_{22}^{x}(cos(k_x)+cos(k_y)) + 2t_{22}^{xx}(cos(2k_x)+cos(2k_y)) + 4t_{22}^{xxyy}(cos(k_x)cos(k_y)),\\
H_{24} &= 4t_{24}^{xy}cos(k_x/2)cos(k_y/2) + 4t_{24}^{xxy}(cos(k_x/2)*cos(3k_y/2)+cos(3k_x/2)cos(k_y/2)).
\end{aligned}
\tag{3}
$$

The hopping parameters are truncated to the fifth-nearest-neighbour site. We get hopping parameters and on-site energies by fitting to the Wannierization result in $k_z=0$ plane, as shown in FIG.S6. The corresponding parameters and their notations are listed in TABLE.S2. The major hopping parameter is t_{11}^{x}, the intra-orbital hopping between two SNN $d_{x^2-y^2}$ orbital, which is in the same energy scale with the dominating intra-orbital hopping between two NN $d_{x^2-y^2}$ orbital in cuprates ($t_{d_{x^2-y^2}}^{NN}$ is about -0.47 in $CaCuO_2$).

As mentioned in our main text, we can transfer the 4×4 TB model into a block-diagonalized matrix with using the glide symmetry:

$$
H_{eff}(\mathbf{k}) = \begin{pmatrix} H_k & 0 \\ 0 & H_{k+Q} \end{pmatrix}, \tag{4}
$$

here H_k is the effective two-band model in our main text and $Q=(\pi,\pi)$. The explict form of H_k is

$$
H_k = \begin{pmatrix} H_{11}+H_{31} & H_{12}+H_{32} \\ H_{21}+H_{41} & H_{22}+H_{42} \end{pmatrix}, \tag{5}
$$

where $H_{\alpha\beta}$ are matrix elements in Eq.3.

Visually, we plot these d-p σ^* Wannier functions in $BaCuS_2$ and $CaCuO_2$, as shown in FIG.S4.(c-e). These Wannier functions are composed of Cu's d-orbitals and coordinated S/O's p-orbitals symmetrically. As the isovalues of isosurfaces in FIG.S4.(c-e) are same, the d-p σ^*-bonding bands are more delocalized in $BaCuS_2$ than that in $CaCuO_2$. As a result, the correlation strength in $BaCuS_2$ should be weaker.

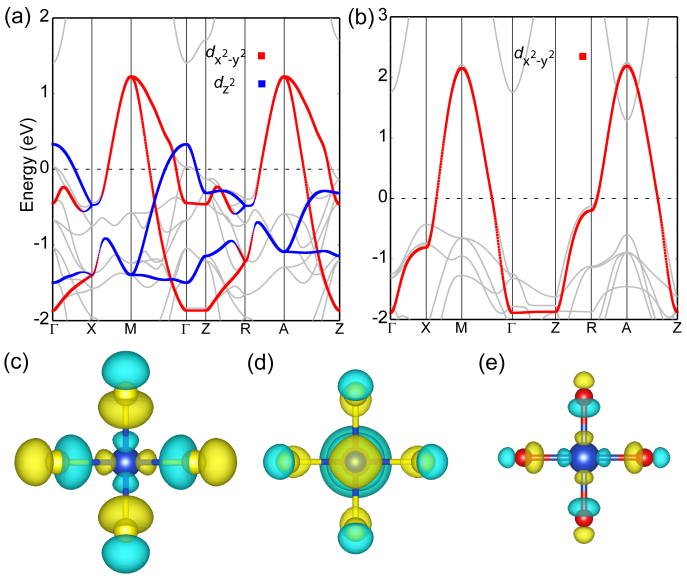

FIG. S4. (a-b) The band structures of (a) $BaCuS_2$ and (b) $CaCuO_2$ calculated by DFT (gray lines) and Wannierizaiton (red/blue dots). The sizes of dots represent the weights of the projection of the d-p σ^* Wannier functions. (c-d) The isosurface of (c) the $d_{x^2-y^2}$-like MLWF and (d) the d_{z^2}-like MLWF in $BaCuS_2$. (e) The isosurface of the $d_{x^2-y^2}$-like MLWF in $CaCuO_2$.

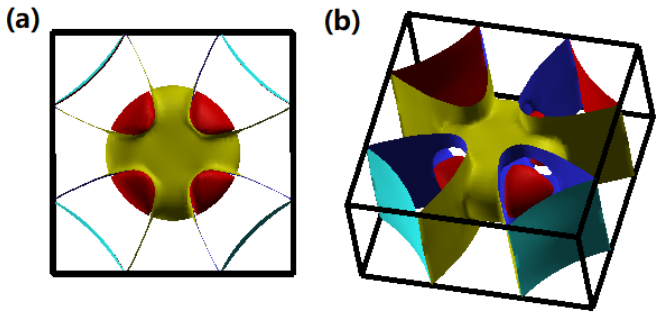

FIG. S5. The Fermi surfaces of $BaCuS_2$ by Wannier fitting with 4 MLWFs from (a) top view and (b) oblique view.

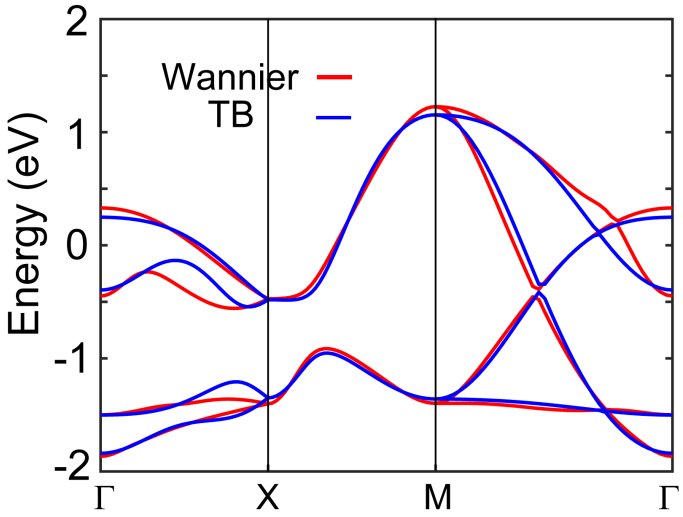

FIG. S6. Comparision of the band structures of $BaCuS_2$ by Wannierizaiton (red lines) and fitted TB model (blue lines).

TABLE S2. The hopping parameters and on-site energies of in-plane TB model for $BaCuS_2$. The energy unit is eV. Here superscript x labels the hopping between two second-nearest-neighbour (SNN) sites along X direction, superscript xx labels the hopping between two forth-nearest-neighbour sites along x direction, superscript xy labels the hopping between two nearest-neighbour (NN) sites along $y = x$ direction, superscript $xxyy$ labels the hopping between two third-nearest-neighbour (TNN) sites along $y = x$ direction, superscript xxy labels the hopping between two fifth-nearest-neighbour sites along $y = x/3$ direction; subscript 1-4 represent Cu_A's $d_{x^2-y^2}$ orbital, Cu_A's d_{z^2} orbital, Cu_B's $d_{x^2-y^2}$ orbital and Cu_B's d_{z^2} orbital, respectively.

ε_1	ε_2	t_{11}^{x}	t_{11}^{xx}	t_{11}^{xxyy}
-0.31	-0.82	-0.28	-0.07	0.15
t_{22}^{x}	t_{22}^{xx}	t_{22}^{xxyy}	t_{12}^{x}	t_{12}^{xx}
0.09	0.003	-0.05	-0.08	0.01
t_{13}^{xy}	t_{13}^{xxy}	t_{24}^{xy}	t_{24}^{xxy}	t_{14}^{xxy}
0.25	-0.03	-0.26	0.02	-0.01

VI. U/J PARAMETERS CALCULATED BY LOCAL SCREENED COULOMB CORRECTION (LSCC) APPROACH

The U/J parameters represent the correlation strength in DFT+U calculations and are often chosen empirically. Here we employ the first-principle LSCC approach[16] to calculate the U/J parameters in layered transition metal compounds $CaCuO_2$, FeSe, $La_3N_3Ni_2B_2$, $BaNiS_2$ and $BaCuS_2$. In LSCC method, the local Coulomb interactions are calculated by using the Yukawa potential, so the U/J should decrease when the system becomes more metallic. Since the U/J is strongly dependent on the muffin-tin radium R_{MT}, we should only compare the U/J with the same pseudopotential. As shown in TABLE.S3, the U/J is larger when AFM order exists in $CaCuO_2$/FeSe. The U/J in $BaNiS_2$ is larger that in $La_3N_3Ni_2B_2$ because the correlation effect are non-negligible in $BaNiS_2$[17, 18] and $La_3N_3Ni_2B_2$ is a typical metal. From this point of view, our results also demonstrate that the correlation in $BaCuS_2$ is weaker than in cuprate $CaCuO_2$.

TABLE S3. The U/J parameters and moments calculated by LSCC method.

LSCC	U (eV)	J (eV)	moment (μ_B)
$CaCuO_2$(AFM)	5.78	1.16	0.478
$CaCuO_2$(NM)	5.74	1.16	0
FeSe(CAFM)	4.88	0.91	3.05
FeSe(NM)	4.75	0.89	0
$La_3N_3Ni_2B_2$	5.49	0.99	0
$BaNiS_2$	5.61	1.01	0
$BaCuS_2$	5.7	1.15	0

VII. METHOD OF RPA CALCULATION

In this section, we explain the formalism of the multiorbital RPA approach[19–23], adopted in the main text. The multiorbital susceptibility is defined as,

$$\chi_{l_1l_2l_3l_4}(\boldsymbol{q},\tau) = \frac{1}{N}\sum_{\boldsymbol{k}\boldsymbol{k}'}\langle T_\tau c^\dagger_{l_3\sigma}(\boldsymbol{k}+\boldsymbol{q},\tau) c_{l_4\sigma}(\boldsymbol{k},\tau) c^\dagger_{l_2\sigma'}(\boldsymbol{k}'-\boldsymbol{q},0) c_{l_1\sigma'}(\boldsymbol{k}',0)\rangle. \tag{6}$$

In momentum-frequency space, the multi-orbital bare susceptibility is given by

$$\chi^0_{l_1l_2l_3l_4}(\boldsymbol{q},i\omega_n) = -\frac{1}{N}\sum_{\boldsymbol{k}\mu\nu} a^{l_4}_\mu(\boldsymbol{k}) a^{l_2*}_\mu(\boldsymbol{k}) a^{l_1}_\nu(\boldsymbol{k}+\boldsymbol{q}) a^{l_3*}_\nu(\boldsymbol{k}+\boldsymbol{q}) \frac{n_F(E_\mu(\boldsymbol{k})) - n_F(E_\nu(\boldsymbol{k}+\boldsymbol{q}))}{i\omega_n + E_\mu(\boldsymbol{k}) - E_\nu(\boldsymbol{k}+\boldsymbol{q})}, \tag{7}$$

where μ and ν are the band indices, n_F is the usual Fermi distribution, l_i $(i = 1, 2, 3, 4)$ are the orbital indices, $a^{l_i}_\mu(k)$ is the l_i orbital component of the eigenvector for band μ resulting from the diagonalization of the tight-binding Hamiltonian H_0 and $E_\mu(\boldsymbol{k})$ is the corresponding eigenvalue. With interactions, the RPA spin and charge susceptibilities are given by

$$\begin{aligned}\chi^{RPA}_s(\boldsymbol{q}) &= \chi^0(\boldsymbol{q})[1-\bar{U}^s\chi^0(\boldsymbol{q})]^{-1},\\ \chi^{RPA}_c(\boldsymbol{q}) &= \chi^0(\boldsymbol{q})[1+\bar{U}^c\chi^0(\boldsymbol{q})]^{-1},\end{aligned} \tag{8}$$

where $\bar{U}^s$ ($\bar{U}^c$) is the spin (charge) interaction matrix,

$$\bar{U}^s_{l_1l_2l_3l_4}(\boldsymbol{q}) = \begin{cases} U & l_1=l_2=l_3=l_4,\\ U' & l_1=l_3\neq l_2=l_4,\\ J & l_1=l_2\neq l_3=l_4,\\ J' & l_1=l_4\neq l_2=l_3,\end{cases} \tag{9}$$

$$\bar{U}^c_{l_1l_2l_3l_4}(\boldsymbol{q}) = \begin{cases} U & l_1=l_2=l_3=l_4,\\ -U'+2J & l_1=l_3\neq l_2=l_4,\\ 2U'-J & l_1=l_2\neq l_3=l_4,\\ J' & l_1=l_4\neq l_2=l_3,\end{cases}. \tag{10}$$

In the main text, we plot the largest eigenvalues of the susceptibility matrix $\chi^0_{l_1l_1l_2l_2}(\boldsymbol{q},0)$ and $\chi^{RPA}_{s,l_1l_1l_2l_2}(\boldsymbol{q},0)$. Within RPA approximation, the effective Cooper scattering interaction on Fermi surfaces is,

$$\Gamma_{ij}(\boldsymbol{k},\boldsymbol{k}') = \sum_{l_1l_2l_3l_4} a^{l_2,*}_{v_i}(\boldsymbol{k}) a^{l_3,*}_{v_i}(-\boldsymbol{k}) Re\Big[\Gamma_{l_1l_2l_3l_4}(\boldsymbol{k},\boldsymbol{k}',\omega=0)\Big] a^{l_1}_{v_j}(\boldsymbol{k}') a^{l_4}_{v_j}(-\boldsymbol{k}'), \tag{11}$$

where the momenta $\boldsymbol{k}$ and $\boldsymbol{k}'$ is restricted to different FSs with $\boldsymbol{k}\in C_i$ and $\boldsymbol{k}'\in C_j$. The orbital vertex function $\Gamma_{l_1l_2l_3l_4}$ in spin singlet channel[24, 25] is

$$\Gamma^S_{l_1l_2l_3l_4}(\boldsymbol{k},\boldsymbol{k}',\omega) = \Big[\frac{3}{2}\bar{U}^s\chi^{RPA}_s(\boldsymbol{k}-\boldsymbol{k}',\omega)\bar{U}^s + \frac{1}{2}\bar{U}^s - \frac{1}{2}\bar{U}^c\chi^{RPA}_c(\boldsymbol{k}-\boldsymbol{k}',\omega)\bar{U}^c + \frac{1}{2}\bar{U}^c\Big]_{l_1l_2l_3l_4}, \tag{12}$$

where χ^{RPA}_s and χ^{RPA}_c are the RPA spin and charge susceptibility, respectively. The pairing strength functional for a specific pairing state is given by,

$$\lambda\big[g(\boldsymbol{k})\big] = -\frac{\sum_{ij}\oint_{C_i}\frac{d\boldsymbol{k}_\parallel}{v_F(\boldsymbol{k})}\oint_{C_j}\frac{d\boldsymbol{k}'_\parallel}{v_F(\boldsymbol{k}')} g(\boldsymbol{k})\Gamma_{ij}(\boldsymbol{k},\boldsymbol{k}')g(\boldsymbol{k}')}{(2\pi)^2\sum_i\oint_{C_i}\frac{d\boldsymbol{k}_\parallel}{v_F(\boldsymbol{k})}\big[g(\boldsymbol{k})\big]^2}, \tag{13}$$

where $v_F(\boldsymbol{k}) = |\nabla_k E_i(\boldsymbol{k})|$ is the Fermi velocity on a given Fermi surface sheet C_i. The pairing vertex function in spin singlet and triplet channels are symmetric and antisymmetric parts of the interaction, that is, $\Gamma^{S/T}_{ij}(\boldsymbol{k},\boldsymbol{k}') = \frac{1}{2}[\Gamma_{ij}(\boldsymbol{k},\boldsymbol{k}') \pm \Gamma_{ij}(\boldsymbol{k},-\boldsymbol{k}')]$.

[1] G. Kresse and J. Furthmüller, Phys. rev. B **54**, 11169 (1996).
[2] G. Kresse and D. Joubert, Phys. Rev. B **59**, 1758 (1999).
[3] J. P. Perdew, K. Burke, and M. Ernzerhof, Phys. Rev. Lett. **77**, 3865 (1996).
[4] A. A. Mostofi, J. R. Yates, Y.-S. Lee, I. Souza, D. Vanderbilt, and N. Marzari, Comput. Phys. Commun. **178**, 685 (2008).
[5] N. Marzari, A. A. Mostofi, J. R. Yates, I. Souza, and D. Vanderbilt, Rev. Mod. Phys. , 1419 (2012).
[6] S. Poncé, E. R. Margine, C. Verdi, and F. Giustino, Computer Physics Communications **209**, 116 (2016).
[7] P. Giannozzi, S. Baroni, N. Bonini, M. Calandra, R. Car, C. Cavazzoni, D. Ceresoli, G. L. Chiarotti, M. Cococcioni, I. Dabo, *et al.*, Journal of physics: Condensed matter **21**, 395502 (2009).
[8] N. Troullier and J. L. Martins, Physical review B **43**, 1993 (1991).
[9] D. Hamann, Physical Review B **88**, 085117 (2013).
[10] M. Schlipf and F. Gygi, Computer Physics Communications **196**, 36 (2015).
[11] P. B. Allen, Physical Review B **6**, 2577 (1972).
[12] P. B. Allen and R. Dynes, Physical Review B **12**, 905 (1975).
[13] D. J. Singh and W. E. Pickett, Phys. Rev. B **51**, 8668 (1995).
[14] Y. Gu, S. Zhu, X. Wang, J. Hu, and H. Chen, Communications Physics **3**, 1 (2020).
[15] F. Zhang and T. Rice, Physical Review B **37**, 3759 (1988).
[16] Y.-C. Wang and H. Jiang, The Journal of chemical physics **150**, 154116 (2019).
[17] Y. Klein, M. Casula, D. Santos-Cottin, A. Audouard, D. Vignolles, G. Feve, V. Freulon, B. Placais, M. Verseils, H. Yang, *et al.*, Physical Review B **97**, 075140 (2018).
[18] D. Santos-Cottin, A. Gauzzi, M. Verseils, B. Baptiste, G. Feve, V. Freulon, B. Placais, M. Casula, and Y. Klein, Physical Review B **93**, 125120 (2016).
[19] N. Berk and J. Schrieffer, Physical Review Letters **17**, 433 (1966).
[20] D. Scalapino, E. Loh Jr, and J. Hirsch, Physical Review B **34**, 8190 (1986).
[21] S. Graser, T. Maier, P. Hirschfeld, and D. Scalapino, New Journal of Physics **11**, 025016 (2009).
[22] A. F. Kemper, T. A. Maier, S. Graser, H.-P. Cheng, P. Hirschfeld, and D. Scalapino, New Journal of Physics **12**, 073030 (2010).
[23] X. Wu, F. Yang, C. Le, H. Fan, and J. Hu, Physical Review B **92**, 104511 (2015).
[24] T. Takimoto, T. Hotta, and K. Ueda, Physical Review B **69**, 104504 (2004).
[25] K. Kubo, Physical Review B **75**, 224509 (2007).